Am J Physiol Cell Physiol 287: C851–C865, 2004.
First published May 12, 2004; 10.1152/ajpcell.00220.2003.

Modeling action potential generation and propagation in NRK fibroblasts

J. J. Torres,[1,2] L. N. Cornelisse,[2,4,*] E. G. A. Harks,[3,*] W. P. M. van Meerwijk,[3] A. P. R. Theuvenet,[3] and D. L. Ypey[3,4,5]

[1]*Institute "Carlos I" for Theoretical and Computational Physics and Department of Electromagnetism and Matter Physics, University of Granada, E-18071 Granada, Spain;* [2]*Department of Medical Physics and Biophysics, University of Nijmegen, 6525 EZ Nijmegen; Departments of* [3]*Cell Biology and* [4]*Cellular Animal Physiology, Institute of Cellular Signaling, University of Nijmegen, 6525 ED Nijmegen; and* [5]*Department of Physiology, Leiden University Medical Center, 2300 RC Leiden, The Netherlands*

Submitted 28 May 2003; accepted in final form 10 May 2004

Torres, J. J., L. N. Cornelisse, E. G. A. Harks, W. P. M. van Meerwijk, A. P. R. Theuvenet, and D. L. Ypey. Modeling action potential generation and propagation in NRK fibroblasts. *Am J Physiol Cell Physiol* 287: C851–C865, 2004. First published May 12, 2004; 10.1152/ajpcell.00220.2003.—Normal rat kidney (NRK) fibroblasts change their excitability properties through the various stages of cell proliferation. The present mathematical model has been developed to explain excitability of quiescent (serum deprived) NRK cells. It includes as cell membrane components, on the basis of patch-clamp experiments, an inwardly rectifying potassium conductance (G_{Kir}), an L-type calcium conductance (G_{CaL}), a leak conductance (G_{leak}), an intracellular calcium-activated chloride conductance [$G_{Cl(Ca)}$], and a gap junctional conductance (G_{gj}), coupling neighboring cells in a hexagonal pattern. This membrane model has been extended with simple intracellular calcium dynamics resulting from calcium entry via G_{CaL} channels, intracellular buffering, and calcium extrusion. It reproduces excitability of single NRK cells and cell clusters and intercellular action potential (AP) propagation in NRK cell monolayers. Excitation can be evoked by electrical stimulation, external potassium-induced depolarization, or hormone-induced intracellular calcium release. Analysis shows the roles of the various ion channels in the ultralong (~30 s) NRK cell AP and reveals the particular role of intracellular calcium dynamics in this AP. We support our earlier conclusion (De Roos A, Willems PH, van Zoelen EJ, and Theuvenet AP. *Am J Physiol Cell Physiol* 273: C1900–C1907, 1997) that AP generation and propagation may act as a rapid mechanism for the propagation of intracellular calcium waves, thus contributing to fast intercellular calcium signaling. The present model serves as a starting point to further analyze excitability changes during contact inhibition and cell transformation.

Hodgkin-Huxley model; intracellular calcium dynamics; L-type calcium conductance; inward rectifier; calcium-activated chloride conductance; gap junctional coupling

NORMAL RAT KIDNEY (NRK) cells are derived from a fibroblastic cell line (clone 49F) that has often been used for the in vitro study of fibroblast functions (2, 13, 27, 28). In previous studies (2, 5), work done in our laboratory has shown that these fibroblasts have excitable properties under certain growth conditions and are able to generate spontaneous or evoked action potentials (APs) with a long-duration plateau (30–60 s), which are propagated by electrical conduction through gap junctional channels between the cells in a confluent monolayer.

So far, channels of an L-type calcium conductance (G_{CaL}) have been shown to be responsible for the upstroke of the AP, and channels of a calcium-activated chloride conductance [$G_{Cl(Ca)}$] have been shown to be responsible for the long-duration plateau. However, ion channels responsible for generation of the resting membrane potential had not yet been identified at the time of these findings, precluding exploration of the mechanisms of NRK cell excitability by modeling. Recently, work in our laboratory (6, 9) demonstrated in voltage-clamp experiments the existence of an inward-rectifier potassium conductance (G_{Kir}) in NRK fibroblasts, consistent with previous experimental work showing the importance of the transmembrane K^+ concentration gradient in generation of the resting membrane potential of these cells (2). This allowed us to start an analysis of NRK cell excitability by modeling the various conductances, including G_{Kir}, to explore whether these conductances suffice to produce excitability and to see how the intracellular calcium dynamics affect AP generation and AP propagation between cells in a monolayer. We have chosen to study and analyze excitability in quiescent NRK cells rather than in density-arrested NRK cells because the latter cells exhibit an extra electrophysiological feature, namely, spontaneous AP firing (pacemaking) (5). This extra feature may result from extra complexity of the excitability mechanism, e.g., the presence of extra membrane conductances for the establishment of an electrical pacemaker mechanism. Starting with the simplest possible model system seemed a logical approach and would also allow us to answer the question whether simple adjustment of the parameters of the model components could, in principle, result in spontaneous firing. This would also help to make predictions for experimental testing of the membrane electrophysiological properties of density-arrested cells. Because the properties of the three active conductances involved [G_{Kir}, G_{CaL}, $G_{Cl(Ca)}$] were not yet fully quantified from voltage-clamp experiments on quiescent NRK cells, we used common or simplified descriptions for these conductances from the literature, as far as available. G_{Kir} was defined as in Ref. 29 for skeletal muscle fibers, and G_{CaL} as in Ref. 24 for bullfrog cardiac pacemaker cells. $G_{Cl(Ca)}$ was defined by assuming simple saturating binding kinetics of intracellular calcium ions to the calcium-sensitive chloride channels as in Ref. 22. Maximal conductance values, reversal potentials, and stationary voltage-dependent properties of G_{Kir} and G_{CaL} were derived from previous voltage-clamp experiments performed in our

* L. N. Cornelisse and E. G. A. Harks contributed equally to this work.
Address for reprint requests and other correspondence: A. P. R. Theuvenet, Dept. of Cell Biology, Institute of Cellular Signaling, Univ. of Nijmegen, Toernooiveld 1, 6525 ED Nijmegen, The Netherlands (E-mail: ATheuv@sci.kun.nl).

The costs of publication of this article were defrayed in part by the payment of page charges. The article must therefore be hereby marked "*advertisement*" in accordance with 18 U.S.C. Section 1734 solely to indicate this fact.

 0363-6143/04 $5.00 Copyright © 2004 the American Physiological Society

Downloaded from http://ajpcell.physiology.org/ by 10.220.32.247 on August 31, 2016

laboratory (9). Intracellular calcium dynamics was simply modeled as a balance between the inflow of calcium ions through G_{CaL} and the efflow by active pumping. A simple calcium buffering mechanism was also included. Before applying the model to the excitability behavior of single and coupled cells, we first checked the validity of the assumed component properties by reconstructing the experimental voltage-clamp records. The geometry of electrical intercellular coupling by gap junctional conductances was made, as a first approximation, in a honeycomb structure (for hexagonal cells), because NRK cells in a monolayer were usually surrounded by six cells. The values of the coupling conductances were derived from coupling conductance estimations in NRK cells (7).

The resulting model reproduced the shapes of APs, which could be evoked in quiescent NRK single cells, cell clusters, and monolayers, and propagation of APs across the monolayer. The model also allowed us to analyze the ionic mechanism of AP generation and to estimate the role of intracellular calcium dynamics in this mechanism. Future versions of the model can be extended with more complex intracellular dynamics (see Refs. 16, 26). This may help us to gain more insight in the mechanism of spontaneous AP firing in density-arrested cells.

MATHEMATICAL MODEL

Single-Cell Model

Using standard Hodgkin-Huxley (HH) type equations, we consider the cell membrane as a single isopotential compartment whose basic equation is given by the membrane voltage equation

$$C_m \frac{dV_m}{dt} = -(I_{CaL} + I_{Kir} + I_{Cl(Ca)} + I_{leak}) \qquad (1)$$

where C_m and V_m represent, respectively, the membrane capacitance and the membrane potential of the cell. The left-hand term of *Eq. 1* represents a capacitive current, while the terms appearing at the right-hand side represent three active ionic currents and a small passive leak current that our laboratory (see Ref. 9) has found to influence the membrane potential dynamics of real NRK fibroblasts. Physiological activation of calcium-sensitive chloride current [$I_{Cl(Ca)}$] requires, besides calcium entry through calcium channels, intracellular calcium regulation by buffering and removal processes upon calcium entry. For this purpose we used a simple calcium dynamics assuming a simple calcium extrusion and buffering mechanism. The conceptual model is represented in Fig. 1*A* and the equivalent electric circuit of the membrane in Fig. 1*B*. Current-clamp simulations with the model cell were carried out by adding an extra constant, I_{CC}, to the right-hand term of *Eq. 1*, representing the applied current-clamp stimulus current. Voltage-clamp stimulation was simulated (see Figs. 2 and 3) by adding (instead of I_{CC}) an extra term, $I_{VC} = G_{ser} \cdot (V_{clamp} - V_m)$, to *Eq. 1*, with V_{clamp} representing the applied (constant) voltage and G_{ser} representing the series conductance between the voltage clamp and the cell membrane. G_{ser} values were derived from previous experiments (9). The description of each of the six basic components of the cell model is as follows.

Leak current. We included leak current (I_{leak}) because it was usually observed in patch-clamp experiments on single cells. The corresponding conductance, G_{leak}, was at least as large as the seal conductance (<1 nS). We then consider

$$I_{leak} = G_{leak} \cdot (V_m - V_{leak}) \qquad (2)$$

where G_{leak} is the (linear) leak conductance. Voltage-clamp experiments reported by Harks et al. (9) suggest that V_{leak} should be set at ~0 mV.

Inward-rectifier potassium current. The presence of inward-rectifier potassium current (I_{Kir}) has been shown in voltage-clamp experiments on isolated NRK fibroblasts (6, 9). An adequate description of this current can be found in Ref. 29 for skeletal muscle fibers and also is used here as

$$I_{Kir} = \bar{G}_{Kir} \cdot \Im(V_m) \cdot (V_m - V_K) \qquad (3)$$

where $\bar{G}_{Kir}$ is the maximal inward-rectifier potassium conductance. I_{Kir} activates at hyperpolarization around and below a potassium equilibrium potential $V_K = -80$ mV. It contributes to both depolarization and repolarization of the AP and is significant in the maintenance of the resting V_m. The sigmoidal function $\Im(V_m)$ represents an instantaneous Boltzmann-type activation curve and is defined in the APPENDIX as a simplified version of the same function in Ref. 29 for a constant external potassium concentration. The parameters appearing in $\Im(V_m)$ were obtained from current-voltage curves derived from voltage-clamp records from real NRK fibroblasts (9).

L-type voltage-gated calcium current. The L-type voltage-gated calcium current (I_{CaL}) is responsible for the fast depo-

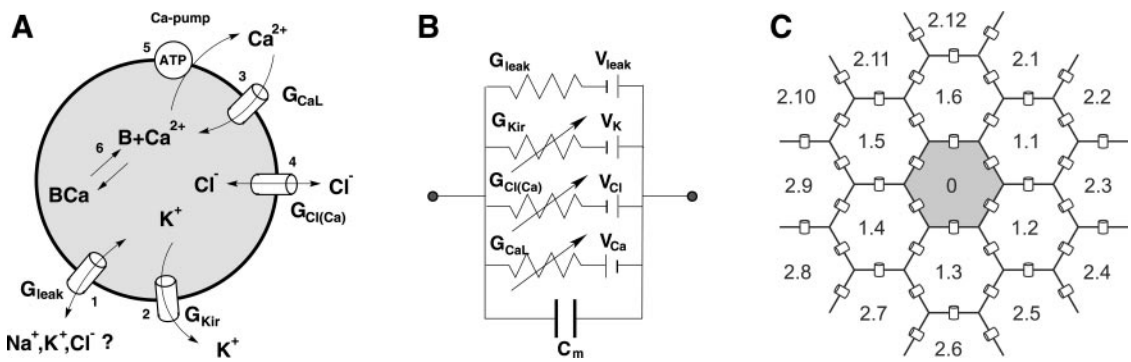

Fig. 1. *A*: conceptual model of a single normal rat kidney (NRK) cell with *components 1–6* (see text for explanation and definitions). *B*: corresponding equivalent circuit. *C*: hexagonal coupling of NRK cells in cell clusters and monolayers. Gap junctional coupling between a cell and its 6 nearest neighbors is symbolized. Intercellular spaces and membrane channels are not represented.

Downloaded from http://ajpcell.physiology.org/ by 10.220.32.247 on August 31, 2016

larization of the membrane at the initiation of an AP. It is expressed in terms of a voltage-dependent conductance with one activation (m) and one inactivation variable (h) multiplied by the HH driving force for calcium ions ($V_m - V_{Ca}$), which is

$$I_{CaL} = \bar{G}_{CaL} \cdot m \cdot h \cdot (V_m - V_{Ca}) \quad (4)$$

where $\bar{G}_{CaL}$ is the maximal calcium conductance (expressed in nS) and V_{Ca} is the reversal potential. The kinetics of the dynamic variables appearing in the definition of I_{CaL} has been taken from a model of the bullfrog cardiac pacemaker cell (24). The main difference between *Eq. 4* and the corresponding equation in Ref. 24 is that we are using a HH driving force instead of a Goldman-Hodgkin-Katz formalism. This allowed us to minimize the number of assumptions and to use the experimentally measured reversal potential of G_{CaL} (9). We have also lowered the time constant for m and h by a factor of 100 to speed up the bullfrog heart I_{CaL} kinetics to that of rat fibroblasts. The dynamics of each of the gating variables ($x = m, h$), in general, can be described by a regular Markov process,

$$\frac{dx}{dt} = \alpha_x(1 - x) - \beta_x x \quad (5)$$

where α_x and β_x are functions of V_m and represent the rates for transition from closed-to-open and from open-to-closed states, respectively. Here, we used the equivalent equation

$$\frac{dx}{dt} = \frac{1}{\tau_x} \cdot (x_\infty - x) \quad (6)$$

where $x_\infty = \alpha_x/(\alpha_x + \beta_x)$ and $\tau_x = 1/(\alpha_x + \beta_x)$ represent the steady-state and time constant, respectively, for each of the channel gates. The dependence of τ_x and x_∞ on V_m is further defined in the APPENDIX. To simulate a U-shaped inactivation curve (24), the inactivation variable h (see Table 2, APPENDIX) is a lumped two-term voltage-dependent variable including both voltage- and calcium-induced inactivation. The first term (a decreasing function) reflects both voltage- and calcium-dependent inactivation at increasing voltages, while the second term (an increasing function) represents the removal of calcium-induced inactivation at increasing voltages, as in Ref. 24. The existence of I_{CaL} has been proven in voltage-clamp experiments on real NRK fibroblasts (5, 9), which provided estimations of activation and inactivation parameters (see Tables 1 and 2, APPENDIX).

Calcium-dependent chloride current. The existence of the three above defined currents is not sufficient to qualitatively reproduce the observed behavior of real NRK fibroblasts. Experiments on monolayers of NRK fibroblasts indicated the presence of a cytosolic calcium-dependent chloride current [$I_{Cl(Ca)}$] in NRK fibroblasts responsible for the maintenance of a long-duration AP plateau near −20 mV (4). In recent voltage-clamp experiments on single quiescent NRK cells and small cell clusters, our laboratory further defined $I_{Cl(Ca)}$ (9). To take into account all these experimental findings, we have completed the model by using the following equation from Puglisi and Bers (22):

$$I_{Cl(Ca)} = \bar{G}_{Cl(Ca)} \cdot \left[\frac{[Ca^{2+}]}{[Ca^{2+}] + K_{Cl(Ca)}}\right] \cdot (V_m - V_{Cl}) \quad (7)$$

where $[Ca^{2+}]$ represents the cytosolic calcium concentration, $\bar{G}_{Cl(Ca)}$ is the maximal chloride conductance, $K_{Cl(Ca)}$ is the half-maximal activation concentration, and V_{Cl} is the chloride equilibrium potential. The dependency of $I_{Cl(Ca)}$ on $[Ca^{2+}]$ implies that, for relatively large values of $[Ca^{2+}]$, this current acts like a leak current that drives the membrane voltage toward V_{Cl}. For low levels of $[Ca^{2+}]$, the effect of $I_{Cl(Ca)}$ is significantly reduced.

Calcium extrusion. Above, we assumed that calcium ions enter the cell through L-type calcium channels. To maintain physiological cytosolic $[Ca^{2+}]$, these ions should be pumped out to the extracellular medium via calcium pumps. Therefore, we also included a calcium dynamics model that represents this calcium extrusion mechanism, first formulated here without the presence of intracellular buffer mechanisms as

$$\frac{d[Ca^{2+}]}{dt} = -\frac{1}{z_{Ca}V_{cell}F} I_{CaL} - V_{pump}^{max} \cdot \left(\frac{[Ca^{2+}]}{[Ca^{2+}] + K_d}\right) \quad (8)$$

The negative sign for the I_{CaL} term arises from the fact that inward calcium current has a negative value. The factor $1/z_{Ca}V_{cell}F$ is a conversion factor that gives the increase of $[Ca^{2+}]$ produced by calcium inflow into the cell via L-type calcium channels. F is the Faraday constant, z_{Ca} is the valence of the calcium ions, and V_{cell} is the cell volume, estimated from the cell morphology (see Table 2, APPENDIX). In *Eq. 8* we have considered a calcium pump system that requires energy in the form of one ATP molecule for each calcium ion pumped out with an affinity of K_d and a maximal pump rate V_{pump}^{max} (15) (see Table 2, APPENDIX). Although the dynamics in *Eq. 8* is rather simple, it is still an important component of the model, for example, for the termination of the long-duration plateau of the AP.

Calcium buffering. In many of the voltage- and current-clamp experiments with real NRK fibroblasts, our laboratory has used nonnatural calcium buffers such as EGTA and BAPTA (9). The buffer molecules bind to free calcium ions with a rate k_{on}, forming a buffer-calcium complex (BCa) that can dissociate also with the rate k_{off} according to the reaction

$$B + Ca^{2+} \underset{k_{off}}{\overset{k_{on}}{\rightleftharpoons}} BCa \quad (9)$$

To include the dynamics of this reaction in the cytosolic calcium dynamics, we then extended *Eq. 8* as follows:

$$\frac{d[Ca^{2+}]}{dt} = k_{off}[BCa] - k_{on}(T_B - [BCa])[Ca^{2+}] - \frac{1}{z_{Ca}V_{cell}F} I_{CaL} - V_{pump}^{max} \cdot \left(\frac{[Ca^{2+}]}{[Ca^{2+}] + K_d}\right); \quad (10)$$

$$\frac{d[BCa]}{dt} = k_{on}(T_B - [BCa])[Ca^{2+}] - k_{off}[BCa]$$

where [B] and [BCa] denote the concentrations of the buffer and the BCa complex, respectively, and T_B denotes the total fixed concentration of buffer molecules, that is, $T_B = [B] + [BCa]$. The same set of equations also can be used for natural intracellular buffering. Rate constants were chosen to obtain a standard dissociation constant $K_d = 0.19$ μM ($k_{on} = 320$ $mM^{-1} \cdot s^{-1}$, $k_{off} = 0.06$ s^{-1}) in the submicromolar order of

Downloaded from http://ajpcell.physiology.org/ by 10.220.32.247 on August 31, 2016

experimental (cf., Ref. 19) and cytoplasmic buffers (cf., Ref. 12). T_B was varied in the 0–100 μM range to investigate the effect of buffer strength, because we used our experimental buffers (EGTA and BAPTA) in that range (9). T_B of natural cytoplasmic buffers is often in the same order (cf., Ref. 12). The standard rate constant k_{on} was chosen at the low side compared with that of experimental buffers (cf., Ref. 19) to be able to investigate the effect of stronger buffering (increased k_{on}).

Coupled-Cell Model

It is known that many fibroblastic cell types in culture, including NRK cells, are electrically well coupled by gap junctional channels (3, 7, 21). These intercellular nonselective ion channels allow the passage of current between neighboring cells when these cells develop a difference in membrane potential. Thus NRK cells in a monolayer form an electrical syncytium over which APs can propagate from cell to cell, as shown by De Roos et al. (2). We have modeled this AP propagation in a monolayer by electrically coupling individual cells with surrounding cells in a hexagonal pattern of a model monolayer of definable size (see Fig. 1*C*). This network geometry approximates the packing of a monolayer of real NRK fibroblasts. Thus the effect of the coupling can be simulated by adding an extra term at the right-hand side of *Eq. 1*, which is

$$I^i_{gj} = \sum_{j\,nn\,i} G^{ij}_{gj}\,(V^i_m - V^j_m) \qquad (11)$$

where G^{ij}_{gj} is the gap junctional electrical conductance between two neighboring cells *i* and *j* and the sum extends over the six nearest neighbors (*nn*) of cell *i*.

The single-cell and coupled-cell models introduced above are schematized in Fig. 1. This is a model of minimal complexity ("minimal model"), constructed to explore whether its basic properties are sufficient to qualitatively reproduce single and coupled NRK cell excitability. Our results show that this is the case. The values of maximal ionic conductances and reversal potentials for all the ionic currents (see APPENDIX) have been taken in accordance with previous experiments (9). Stationary activation and inactivation parameters [V_m of half-maximal (in)activation and steepness factors] are in the range of values found by Harks et al. (9) in real NRK fibroblasts. All information about model details such as transition rates and other functions or parameters of the model is summarized in the APPENDIX.

The dynamical system described by *Eqs. 1–11* was numerically integrated in a regular personal computer, using fourth-order Runge-Kutta with time step $\Delta t = 10^{-5}$, and programmed with standard C++. Stable-start values for the dynamical variables used in the simulations are as follows: $V_m = -73.4$ mV, $m = 10^{-5}$, $h = 0.99$, cytoplasmic $[Ca^{2+}] = 20$ nM, and [BCa] = 0 nM. The starting baseline conditions were the same for both current-clamp and voltage-clamp simulations, and the baseline conditions for the successive current or voltage steps were those obtained after a very long-duration transient (sufficient to avoid possible non-steady-state effects) after the voltage or current step.

RESULTS

Single-Cell Voltage-Clamp Properties

The model described by *Eqs. 1–10* for a single NRK cell is able to reproduce the main features of voltage- and current-clamp experiments on real NRK fibroblasts. Figure 2 shows a set of illustrative voltage-clamp simulations on the cell model including buffering of cytosolic calcium for different values of the total amount of buffer, T_B. The numerical experiment simulates the effect of an EGTA- or BAPTA-like buffer in the pipette solution in real voltage-clamp experiments. Figure 2 illustrates the characteristic properties of the total current when the membrane voltage is clamped with increasing voltage steps from −120 to +20 mV. For large, negative voltage steps, the total current is mainly carried by an inward-rectifier potassium current (constant negative current records), because this current is activated by hyperpolarization. For voltage steps above −40 mV, I_{CaL} becomes activated whereas I_{Kir} becomes deactivated. The total current then shows the main features of I_{CaL}, which is an initial rapid increase in negative current (activation) followed by a slower decrease (inactivation). This is best visible in the current record shown in Fig. 2, *bottom right*, where I_{CaL} is the only time-dependent current around 0 mV.

An important consequence of I_{CaL} is an increase of the cytosolic calcium concentration. For voltage steps higher than 0, this is reflected as the appearance of an outward increasing current, $I_{Cl(Ca)}$. This current is large if $[Ca^{2+}]$ is high and small if $[Ca^{2+}]$ is low, as can be shown by varying T_B. Thus, for relatively small T_B (~4 μM), the cytosolic calcium was hardly buffered, and therefore $I_{Cl(Ca)}$ was high (Fig. 2, *top left*). For relatively high T_B (for example, $T_B = 100$ μM), the cytosolic calcium was almost fully buffered, and then $I_{Cl(Ca)}$ was zero (Fig. 2, *bottom right*). For this situation, no time-dependent outward current is observed and only I_{CaL} appears for large, positive voltage steps. After comparison with experimental recordings presented by Harks et al. (9), it appears that the model behavior is qualitatively similar to that observed in voltage-clamp experiments on real NRK fibroblasts. Those experiments were performed with EGTA in the pipette solution, which is widely used as a calcium buffer. In the presence of high EGTA concentrations (3.5 mM), most of the current records presented by Harks et al. (9) do not show a high outward $I_{Cl(Ca)}$. By lowering the EGTA concentration in the pipette solution (to 100 μM), calcium buffering was decreased and a large outward $I_{Cl(Ca)}$ was measured in single cells. Quantitative differences in effectively blocking T_B values between simulation and experiment may be due to differences in the buffering kinetics, because extra simulations showed that 10× increased k_{on} values made $T_B = 20$ μM, a value almost fully suppressive for $I_{Cl(Ca)}$ (provided inward calcium currents did not saturate the buffer), whereas 0.1× decreased k_{on} values increased the $I_{Cl(Ca)}$.

In voltage-clamp experiments on clusters of cells, the small $I_{Cl(Ca)}$ currents of the individual cells add up (see *Voltage-clamp properties of small cell clusters*), giving rise to larger outward currents. However, when a strong intracellular calcium buffer (with large k_{on}) was added (BAPTA), these outward currents disappeared, demonstrating that the outward current is a result of an intracellular calcium transient as in the model. Thus various effects of intracellular buffering by EGTA

Downloaded from http://ajpcell.physiology.org/ by 10.220.32.247 on August 31, 2016

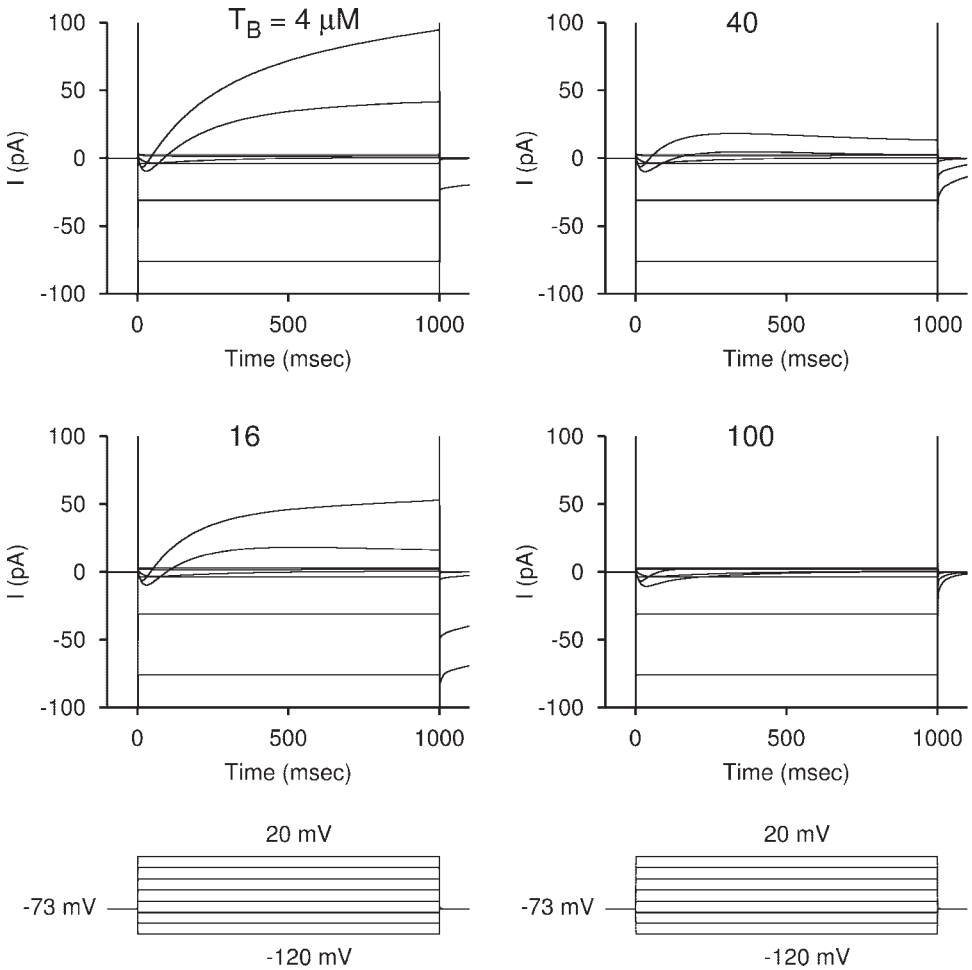

Fig. 2. Voltage-clamp experiments on a NRK fibroblast single-cell model including buffering at different values for the total buffer amount T_B = 4, 16, 40, and 100 μM, respectively; for the rate at which buffer molecules bind to free calcium ions, k_{on} = 320 $mM^{-1} \cdot s^{-1}$; and for the rate at which the buffer-calcium complex (BCa) dissociates, k_{off} = 0.06 s^{-1}. Other parameter values are as defined in APPENDIX. Applied voltage-step protocols are shown at *bottom*. The holding potential of −73 mV has been taken as equal to the resting membrane potential of the cell. The initial sharp spike in the records is the capacitive current transient caused by the presence of the series conductance (G_{ser}) of 50 nS. The lowest current was recorded at −120 mV and the highest at +20 mV. Voltage increments between records were +20 mV.

and BAPTA can be described, at least qualitatively, by choosing sets of buffer parameters in *Eq. 10*.

Voltage-Clamp Properties of Small Cell Clusters

Patch-clamp experiments on small cell clusters of NRK cells show current responses to voltage-clamp steps similar to those in single-cell experiments (9). The main difference seems to be that the amplitude of the recorded currents is higher for the cell cluster than for the single cell, because currents are also being recorded from the cells coupled to the patched cell. Because the currents from single NRK cells are very small, in our experimental studies we used voltage-clamp records from cell clusters to improve resolution. However, slower capacitive transients due to the overall coupling with the neighboring cells are visible in the records. This could imply worsened voltage-clamp conditions because of the gap junctional resistance serving as an access resistance to the cells surrounding the patched cell. We used the present model to evaluate the voltage-clamp conditions in patch-clamp experiments on small cell clusters. We considered a cluster of one single cell coupled to six neighbor cells in a hexagonal geometry with different gap junctional conductances G_{gj} and included the effect of medium-strong buffering of calcium (T_B = 20 μM) in all cells. Figure 3 shows the main results. For G_{gj} = 0 nS, the records look like those from a single NRK cell experiment. The sharp needles at the up and down steps of the test voltage are the capacitive transients with peaks and time constants determined by the series resistance (R_{ser}) and the $R_{ser} \times C_m$ values, respectively (R_{ser} = 20 MΩ as a worst case, C_m = 20 pF). The voltage-clamp conditions are good for the small currents measured, because the voltage drop over R_{ser} is <2 mV (20 MΩ × 100 pA). For increasing G_{gj}, the currents increase because of the contributions from the surrounding cells, but the capacitive current transients widen, indicating the delayed charging of the coupled cells to the applied voltage. The worst coupling (G_{gj} = 1 nS) has the slowest capacitive current transient, and the best coupling (G_{gj} = 60 nS) has the fastest. For ideal voltage clamp, one would expect currents seven times larger in a seven-cell cluster compared with current in a single cell. With G_{gj} = 60 nS, this turned out to be the case for I_{CaL} (2% error in the estimation of I_{CaL} at −20 mV). G_{gj} = 60 nS corresponds to a total coupling conductance to the surrounding cell ring (G_{tgj}) of 360 nS (R_{tgj} ~3 MΩ). In that case, R_{ser} = 20 MΩ has become limiting in recording current from the surrounding ring, giving an underestimation of the inward-rectifier current at −120 mV of 24%. Thus, although the reliable measurability of small currents (e.g., I_{CaL}) in a small (7 cell) NRK cell cluster may be much improved, the measurement of maximal values of the larger currents [I_{Kir} and sometimes $I_{Cl(Ca)}$] is less reliable than in single cells, depending on the sum of R_{ser} and R_{tgj}.

Downloaded from http://ajpcell.physiology.org/ by 10.220.32.247 on August 31, 2016

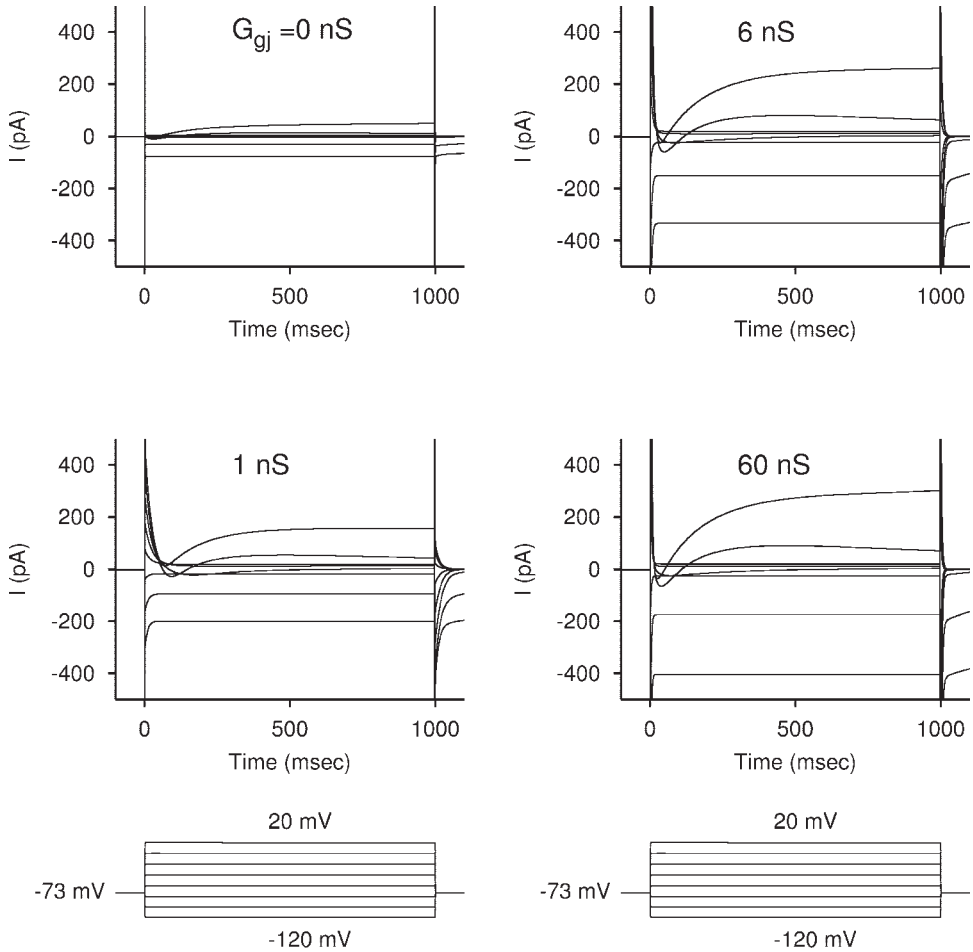

Fig. 3. Voltage-clamp experiments in a cluster of 7 NRK model cells for different degrees of gap junctional coupling (G_{gj}) of 0, 1, 6, and 60 nS, as indicated. Buffer parameters were T_B = 20 μM, k_{on} = 320 $mM^{-1}\cdot s^{-1}$, and k_{off} = 0.06 s^{-1}. Series conductance G_{ser} = 50 nS (series resistance R_{ser} = 20 MΩ). Other parameter values are as defined in APPENDIX. Applied voltage step protocols are shown at *bottom*.

Excitability of Single Cells

The model cell is able to generate APs similar to those measured in real NRK fibroblasts (9). To demonstrate the excitability properties of our single-cell model, we first used the standard buffer parameters in *Eq. 10*: T_B = 20 μM, k_{on} = 320 $mM^{-1}\cdot s^{-1}$, and k_{off} = 0.06 s^{-1}. Figure 4*A* shows that upon stimulation with positive current pulses of sufficient strength, the membrane potential quickly changes from its resting value toward more positive values. This depolarization is produced in the model mainly by a combination of an increasing inward I_{CaL} and a decreasing outward I_{Kir}, as illustrated in Fig. 4*B*, where the individual currents have been plotted during an AP. After activation, inactivation of I_{CaL} contributes to the overall repolarization process of the AP. I_{CaL} generates a significant influx of calcium ions that transiently increases $[Ca^{2+}]$ in the cytosol. The elevation of $[Ca^{2+}]$ in the cytosol (see Fig. 4*C*) activates $I_{Cl(Ca)}$, which significantly contributes to the initial repolarization by pulling the membrane voltage toward V_{Cl} = −20 mV. The end of the calcium transient produces a decreasing $I_{Cl(Ca)}$ such that the membrane becomes subject to the repolarizing effect of I_{Kir}. As a consequence, the membrane drops from the voltage plateau at −20 mV to the resting potential near −70 mV (cf., Fig. 4, *B* and *C*). At this voltage, I_{Kir} remains active and I_{CaL} recovers from inactivation for repeated generation of an AP. The effect of I_{Kir} is to maintain the voltage near the resting membrane potential by opposing the depolarizing effect of I_{leak} at low voltages. This effect is shown in Fig. 4*B*, where I_{leak} and I_{Kir} are the most important currents under resting conditions. $I_{Cl(Ca)}$ is very close to zero just before the AP, because there is practically no baseline inflow through the G_{CaL} channels. Thus $I_{Cl(Ca)}$ contributes little or nothing to the resting membrane potential in our model. Separate simulations showed, however, that if some calcium leak were allowed, to generate a small baseline $[Ca^{2+}]$, then $I_{Cl(Ca)}$ would have a depolarizing effect on the resting membrane potential. Nevertheless, it was possible to choose for a given G_{Kir} combinations of G_{leak} and $G_{Cl(Ca)}$ with maintained resting membrane potential and excitability. In the absence of intracellular calcium buffering, the single-cell model AP is much longer (see Fig. 5*B1* for another method of stimulation) because of an extended intracellular calcium transient (see Fig. 5*B2*). This relationship is further explained in *Potassium pulse induced single-cell APs*.

Reproducing excitability required a 12-mV higher separation of the activation and inactivation curve: half-activation ($V_{1/2}$ of m_∞) and half-inactivation ($V_{1/2}$ of h_∞) values −10 and −45 mV, respectively, instead of the experimental values −15 and −37 mV reported by Harks et al. (9), respectively. This may indicate imperfectness of the Rasmusson model and/or imprecise parameter values of the other components of the model.

Downloaded from http://ajpcell.physiology.org/ by 10.220.32.247 on August 31, 2016

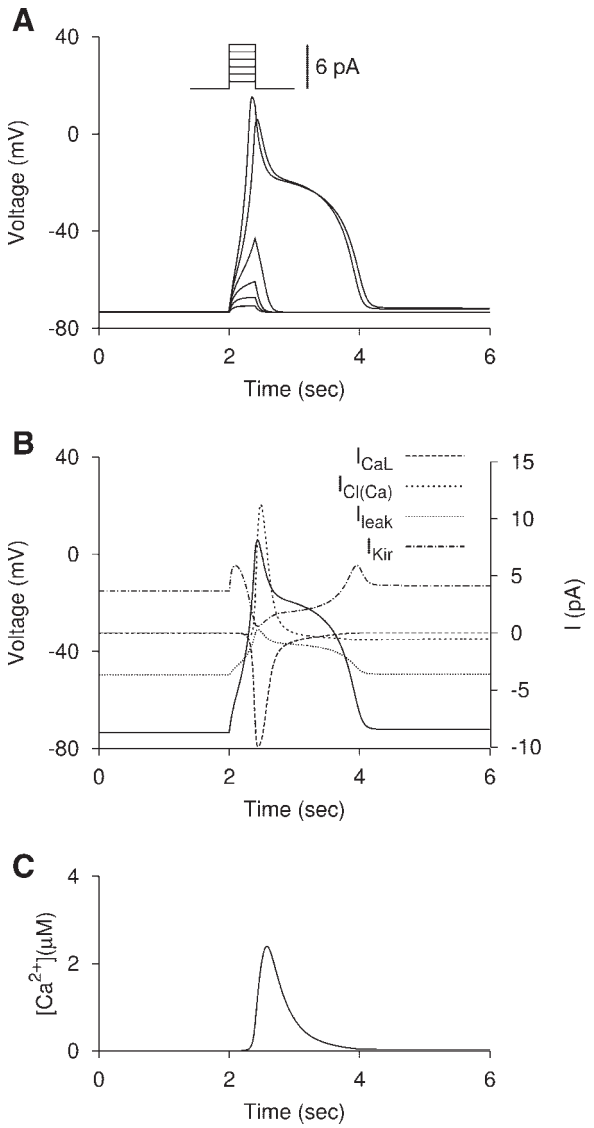

Fig. 4. Current-clamp experiments in an isolated NRK fibroblast model cell. *A*: subthreshold responses and action potentials (APs) generated upon different current steps of 1–6 pA and of 400-ms duration. The simulated passive behavior of the cell membrane for a current injection of 1 pA allowed for a calculation of the membrane resistance $R_m = 2.54$ GΩ and $\tau = R_m C_m = 50.8$ ms. These values are comparable to those obtained experimentally from NRK cells (9). *B*: time courses of the currents involved (dotted and dashed lines) in the NRK fibroblast cell model to illustrate their relative importance during AP generation by a 5-pA pulse (solid line). *C*: intracellular calcium transient ($[Ca^{2+}]$) during the AP. Buffer parameters are $T_B = 20$ μM, $k_{on} = 320$ $mM^{-1}\cdot s^{-1}$, and $k_{off} = 0.06$ s^{-1}. Other parameter values are as defined in APPENDIX.

The role of calcium buffering in shaping the AP was further investigated by changing the buffer parameters. For example, reducing T_B to 6 μM made buffering weaker, causing a larger and longer intracellular calcium transient and larger AP duration (~8 s). A plot of the various currents during this long AP showed that there was a small sustained I_{CaL} during the AP plateau but that this sustained current was smaller than the maximal calcium extrusion rate, thus allowing the eventual complete clearance of accumulated calcium. The effect of T_B is further described for external potassium (see *Potassium pulse-induced single-cell APs*) and internal calcium pulse-evoked APs (see *Cytosolic calcium pulse-induced single-cell APs*).

Alternatively, calcium buffering could be manipulated by changing k_{on} at a constant standard T_B (20 μM). A 10× increase in k_{on} created more experimental bufferlike properties and almost fully suppressed the intracellular calcium transient. This caused the AP to loose its initial rapid $I_{Cl(Ca)}$-induced repolarization and to repolarize more slowly, mainly determined by the G_{CaL} inactivation and the G_{Kir} activation mechanism. A 0.1× decrease in k_{on} created more natural bufferlike properties and caused a higher and longer intracellular calcium transient and a correspondingly longer AP. The effect of a rapidly acting buffer on the AP indeed looks like the effect of BAPTA on the monolayer AP (see Ref. 9).

Potassium Pulse-Induced Single-Cell APs

We have also studied the ability of the NRK single-cell model to generate APs upon short-time exposure to a high concentration of external potassium. In this way, a propagating AP with a long-duration plateau could be evoked in NRK monolayers under conditions in which external calcium ions were replaced by strontium ions (2, 9). We simulated the effect of K^+ pulses on the membrane by changing V_K from −80 to 0 mV for the duration of the pulse (~400 ms). Figure 5 shows our main results for two different calcium buffering conditions. First, we observed that the NRK single-cell model can generate APs with the same properties upon current injections and potassium pulses (cf., Fig. 5*A1* with Fig. 4). Second, removal of intracellular buffering from the model cell causes a tremendous (~20×) increase in the duration of the AP (Fig. 5*B1*). At an intermediate T_B value of 6 μM, an intermediate AP duration of ~19 s was obtained. Thus Fig. 5 also illustrates one of the predictions of our model, which is the correlation between duration of the AP plateau and that of the intracellular calcium transient (Fig. 5, *A2* and *B2*).[1] This correlation would apply for any factor affecting the duration of the intracellular transient, whether by changes of the inflow of calcium through plasma membrane channels or by changes in intracellular calcium release or changes in intracellular buffering. One example of such a factor is the exact shape of the calcium inflow as determined by the G_{CaL} properties, as prescribed by the Rasmusson model for this conductance. If we remove the calcium inactivation removal term, the AP duration is less lengthened in Fig. 5*B* because of reduced calcium inflow.

Cytosolic Calcium Pulse-Induced Single-Cell Action Potentials

Excitation of NRK cell monolayers by certain hormones (e.g., bradykinin) is the consequence of calcium release from intracellular stores evoked by those hormones (2). The presumed mechanism of this excitation was membrane depolarization via calcium-activated chloride channels. We were therefore interested to know whether such a depolarization by a rise in the internal $[Ca^{2+}]$ could also cause excitation of our NRK cell model. An increasing $[Ca^{2+}]$ would activate $I_{Cl(Ca)}$, thereby depolarizing the membrane beyond the threshold for I_{CaL} and causing the generation of an AP. To investigate this

[1] The shape of the calcium transient in the absence of calcium buffering may not be realistic because of the simple calcium dynamics we are considering.

Downloaded from http://ajpcell.physiology.org/ by 10.220.32.247 on August 31, 2016

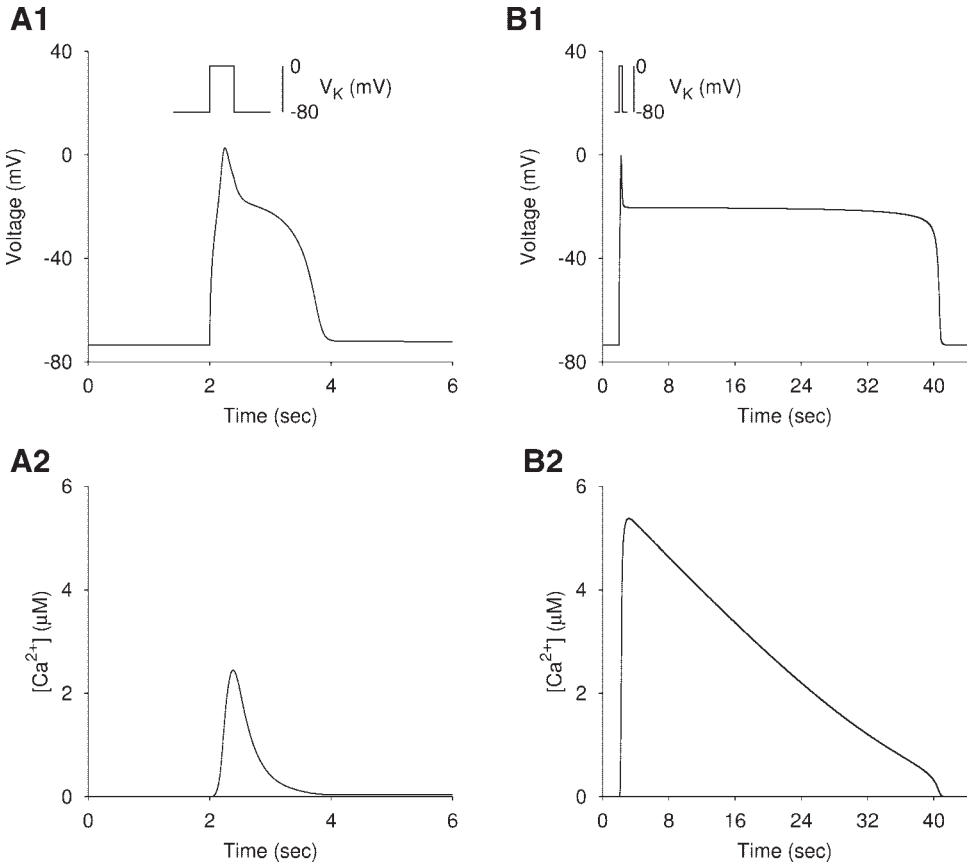

Fig. 5. Excitation of the NRK fibroblast single-cell model by a short external potassium pulse (*A1* and *B1*) and the corresponding variation produced on the intracellular $[Ca^{2+}]$ (*A2* and *B2*) for 2 buffering conditions. This pulse was simulated by changing the potassium equilibrium potential V_K from −80 mV to 0 mV over a duration of 400 ms at 2 different buffering conditions (*A* and *B*). Buffer parameters in *A* are $T_B = 20$ μM, $k_{on} = 320$ $mM^{-1}\cdot s^{-1}$, and $k_{off} = 0.06$ s^{-1}; in *B*, $T_B = 0$ μM.

possibility, we applied intracellular calcium pulses to the cell. The NRK single-cell model was indeed able to produce APs upon application of calcium pulses to the cytosol. We increased $[Ca^{2+}]$ in the cytosol by adding a positive constant term of 0.01 $mM\cdot s^{-1}$ to the right-hand side of the first part of *Eq. 10*. Figure 6 shows the AP generated in a NRK single-cell model under two different calcium buffering conditions. The results are similar to those with potassium pulses (Fig. 5), except that there is no significant initial overshooting spike in the AP. One reason for this difference must be that the effect of I_{CaL} on membrane potential now acts against a background of $I_{Cl(Ca)}$, which is not the case during stimulation with potassium pulses (and electrical stimulation; see Fig. 4).

Single-Cell Excitability with Strontium

Patch-clamp experiments on AP generation in NRK monolayers have been performed by substituting the calcium ions in the extracellular medium with strontium ions to improve excitability (9). By using this procedure, I_{CaL} in voltage-clamp experiments on living single cells was increased by a factor of 2, and moreover, strontium decelerated inactivation of L-type calcium channels (9). To take into account these two effects of strontium on I_{CaL} and to be able to generate APs in the NRK single-cell model in the presence of strontium, we changed $G_{CaL} = 0.5$ nS in the model to $G_{SrL} = 1$ nS. Furthermore, we changed the second term in the equation for *h* (steady-state inactivation; see Table 2, APPENDIX) to

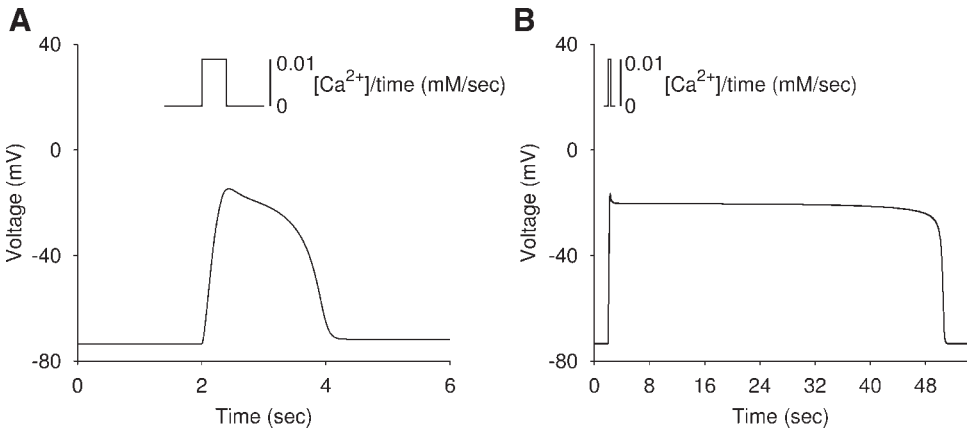

Fig. 6. Excitation of the NRK fibroblast single-cell model by an intracellular calcium pulse for 2 buffering conditions. This pulse was simulated by increasing the intracellular $[Ca^{2+}]$ by 0.01 mM/s over a duration of 400 ms at 2 different buffering conditions (*A* and *B*). Buffer parameters in *A* are $T_B = 20$ μM, $k_{on} = 320$ $mM^{-1}\cdot s^{-1}$, and $k_{off} = 0.06$ s^{-1}; in *B*, $T_B = 0$ μM.

Downloaded from http://ajpcell.physiology.org/ by 10.220.32.247 on August 31, 2016

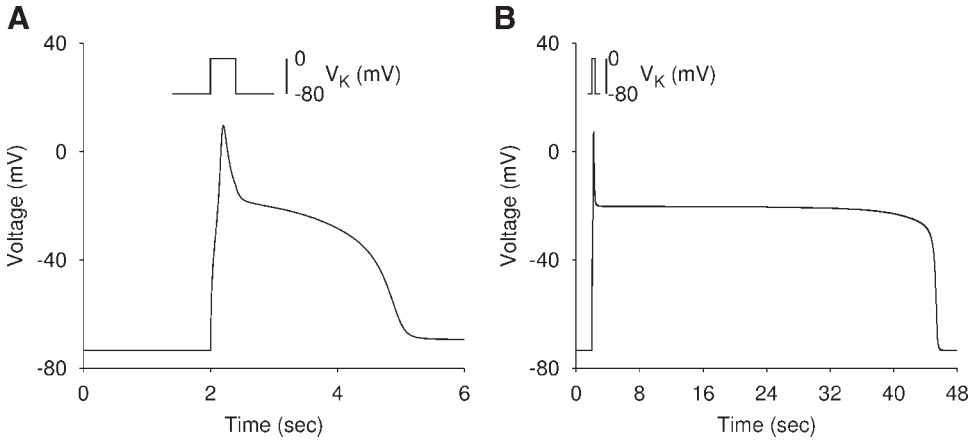

Fig. 7. Excitation of the NRK fibroblast single-cell model by a potassium pulse with strontium in the external medium for 2 buffering conditions (*A* and *B*). This pulse was simulated by changing the V_K from −80 mV to 0 mV over a duration of 400 ms at 2 different buffering conditions. Buffer parameters in *A* are T_B = 20 μM, k_{on} = 320 $mM^{-1} \cdot s^{-1}$, and k_{off} = 0.06 s^{-1}; in *B*, T_B = 0 μM.

0 (no removal of calcium-induced inactivation of the channel in the presence of strontium). To maintain excitability with full repolarization, we had to shift the $V_{1/2}$ from −45 to −49.3 mV, probably to compensate for the extra inflow of strontium (compared with calcium) during the AP. Figures 7 and 8 show AP generation in a NRK single-cell model by $[K^+]$ and $[Ca^{2+}]$ pulses, respectively, in the presence of 2 mM external strontium, for two different buffering conditions. The results are essentially the same as for calcium, except that the initial AP spikes are more pronounced because of a stronger inward current induced by strontium. For simplicity, we assumed here that the strontium ions only affected the calcium channel properties (see Ref. 9) and that intracellular strontium handling (buffering and extrusion) occurred in the same way as calcium handling. The latter assumption is supported by the observation that the duration of the strontium AP is not very different from that of the calcium AP (2).

Excitability of Small Cell Clusters

Our group has also performed several current-clamp simulation experiments in the presence of external calcium on small cell clusters consisting of seven model cells (1 cell in the center of the cluster and 6 neighboring cells) coupled via gap junctions with conductance G_{gj}, because small clusters of real NRK fibroblasts appeared to be excitable (see Ref. 9). These simulations were also useful as a preparation for the more time-consuming simulations on large monolayers. Figures 9 and 10 show our main results. In the experiment shown in Fig. 9, we applied increasing current steps in the cell in the center of such a seven-cell cluster, while the electrical conductance between the cells was G_{gj} = 6 nS. This resulted in a physiological coupling conductance between the center cell and the surrounding ring of ~36 nS (7). Figure 9 shows that an AP was evoked in the cluster for current steps above 32 pA. In addition, we observed almost complete synchrony between the membrane potential change in the center cell and that in the neighboring cells due to the high electrical conductance of the gap junctions. As a consequence, to evoke an AP, it was necessary to apply much larger current steps in the cluster than in a single cell (see Fig. 4). In the experiment shown in Fig. 10, we explored the ability of the model to produce AP propagation in a small cluster of model cells at various coupling strengths. Using the same current step in all experiments (I_{step} = 32 pA), we observed that depending on the strength of the gap junctional electrical conductance, the AP generated in the center of the cluster was able to propagate to the neighboring cells. A relatively small G_{gj} (~0.3 nS) was already sufficient for AP propagation in these high-resistance NRK cells (R_m > 1 GΩ). Figure 10 also shows that the delay between AP firing in the center cell and that in a neighboring cell (AP transfer time) was smaller when G_{gj} was increased, consistent with an accelerated AP conduction for increased values of G_{gj}.

Excitability and Wave Propagation in a Monolayer of NRK Fibroblasts

Finally, we simulated AP generation in a quiescent NRK monolayer with strontium in the extracellular medium. We

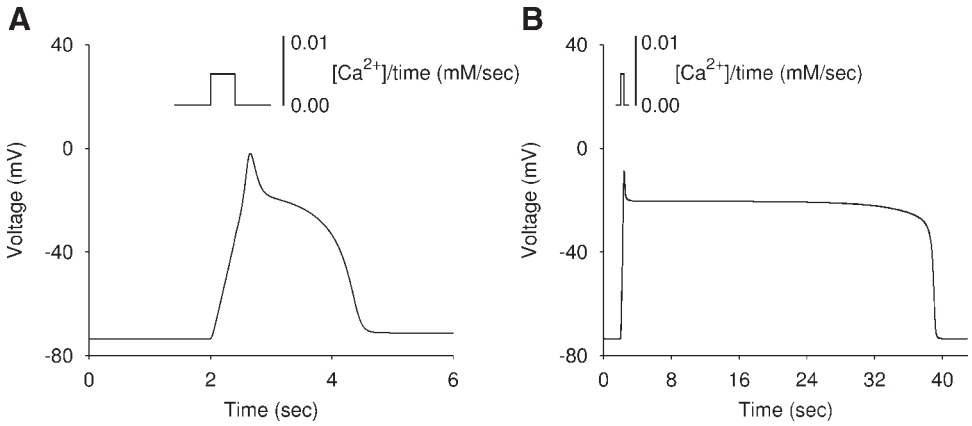

Fig. 8. Excitation of the NRK fibroblast single-cell model by an intracellular calcium pulse with strontium in the external medium for 2 buffering conditions. This pulse was simulated by increasing the intracellular $[Ca^{2+}]$ by 5 μM/s over a duration of 400 ms at 2 different buffering conditions (*A* and *B*). Buffer parameters in *A* are T_B = 20 μM, k_{on} = 320 $mM^{-1} \cdot s^{-1}$, and k_{off} = 0.06 s^{-1}; in *B*, T_B = 0 μM.

Downloaded from http://ajpcell.physiology.org/ by 10.220.32.247 on August 31, 2016

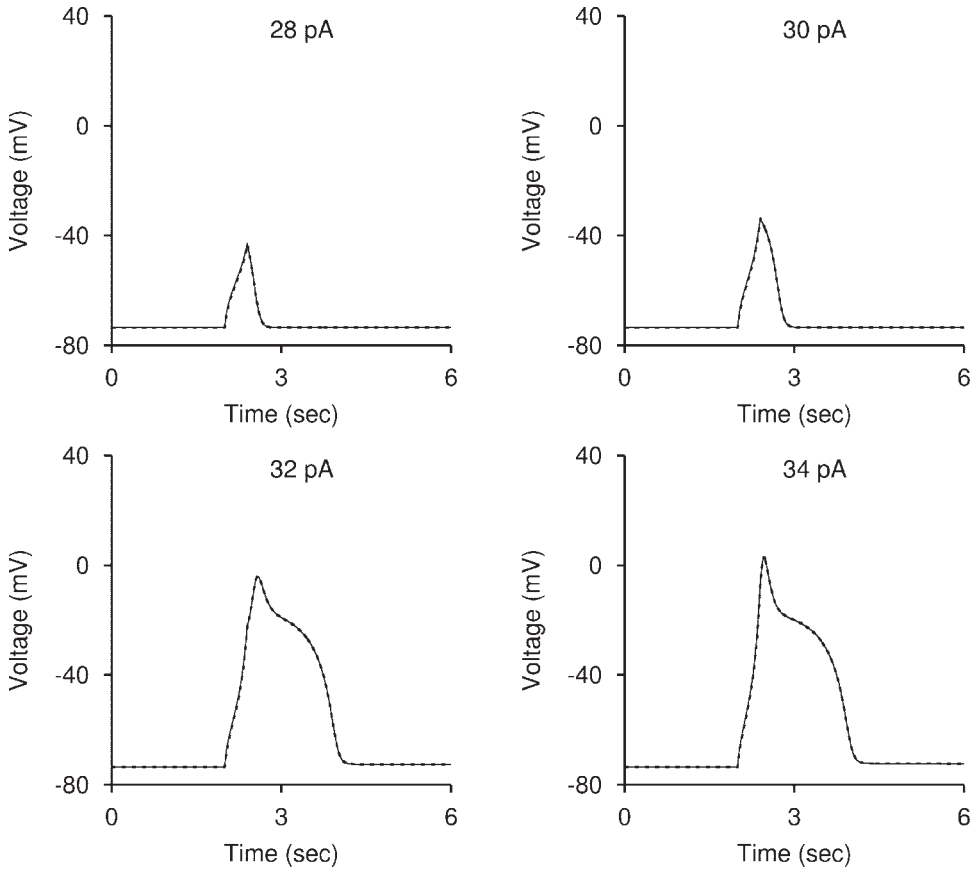

Fig. 9. Current-clamp experiments in a cluster of 7 NRK fibroblast model cells. Current steps of various strengths were applied to the center cell, which is coupled with the surrounding 6 cells by gap junctions of strength G_{gj} = 6 nS. Each panel represents 2 superimposed responses: 1 is recorded in the center cell of the cluster (solid line), and the other is recorded in 1 of the surrounding cells (dashed line, hardly visible at this coupling strength). The 4 different current steps are indicated in pA. Buffer parameters for all cells in the cluster are T_B = 20 μM, k_{on} = 320 $mM^{-1} \cdot s^{-1}$, and k_{off} = 0.06 s^{-1}. Other parameter values are as defined in APPENDIX.

used a 7 × 7-cell network with hexagonal geometry (see Fig. 1*C*) and applied a potassium stimulus to a cluster of 19 cells in the center of such a network, because stimulations of smaller central areas did not work. As we explained earlier, this is equivalent to changing the V_K from −80 to 0 mV in all 19 of these cells and leaving the rest of the cells in the network unaltered. Buffering was left out (T_B = 0) to show the effect of coupling in a monolayer for the most simple AP mechanism. Figure 11 shows the main results. The electrical responses generated in two cells of the network, one in the center of the network, and therefore in the stimulation area, and the other at the border, outside the stimulation area. Figure 11 shows AP generation and propagation through the network for different gap junctional strengths. Two main conclusions arise. First, the delay between the AP of the cell in the center and that of a cell at the border decreases with increasing G_{gj}. At G_{gj} = 0.5 nS, the delay is 220 ms, whereas at G_{gj} =10 nS, it is 7 ms, meaning that the velocity of wave propagation from the center to the border of the network also increases with G_{gj}. Second, the height of the initial peak and the duration of the AP clearly depend on electrical coupling. AP peak and duration decrease upon the establishment of coupling by G_{gj} = 0.5 nS but subsequently increase again upon a further increase in G_{gj}. The fact that AP peak and duration change in the same direction indicates that AP duration changes are caused by changes in the size of the inward calcium current, causing changes in duration of the intracellular calcium pulse and associated $G_{Cl(Ca)}$ activation. These effects can be interpreted in terms of coupling-dependent changes in loading of the central excited cells by the surrounding nonstimulated cells. At weak coupling (0.5 nS), the AP delays in subsequent cell excitations are relatively long (~50 ms) compared with the used time constant of inactivation (~250 ms in the range of activation), causing partial inactivation of the calcium conductance during the depolarization phase of the AP. At stronger coupling, loading and partial inactivation diminish again when the APs become almost synchronized. Whatever the mechanism of the coupling-dependent AP peak amplitude and duration, these simulation results show how the excitability of a larger ensemble of excitable cells such as an NRK cell monolayer can depend on the strength of electrical coupling between the cells.

By direct comparison with similar kinds of experiments reported by Harks et al. (9), we can show the good agreement of our simulated AP generation in a monolayer with AP generation in real NRK monolayers in the quiescent state. The model is able to reproduce both the shape of the AP and the size of the long-duration plateaus (~30 s in this experiment). This could mean that intracellular calcium buffering in the cells of an NRK cell monolayer is not strong, but another possibility is that intracellular calcium release, not included here, lengthens the calcium transient in NRK cells.

Finally, Fig. 12 shows a series of color snapshots reflecting the propagation of the AP over a network of 9 × 9 cells (with speed v ~1.5 mm/s or equivalently, ~90 cells/s) where dark blue color represents the region of lowest voltage (approximately resting membrane potential) and red color represents the region of highest voltage (AP peak). The potassium stimulus was applied to a central area of 19 cells. T_B was chosen to be smaller (9 μM) than in the above-described simulation experiments on single cells and small cell clusters (20 μM) to

Downloaded from http://ajpcell.physiology.org/ by 10.220.32.247 on August 31, 2016

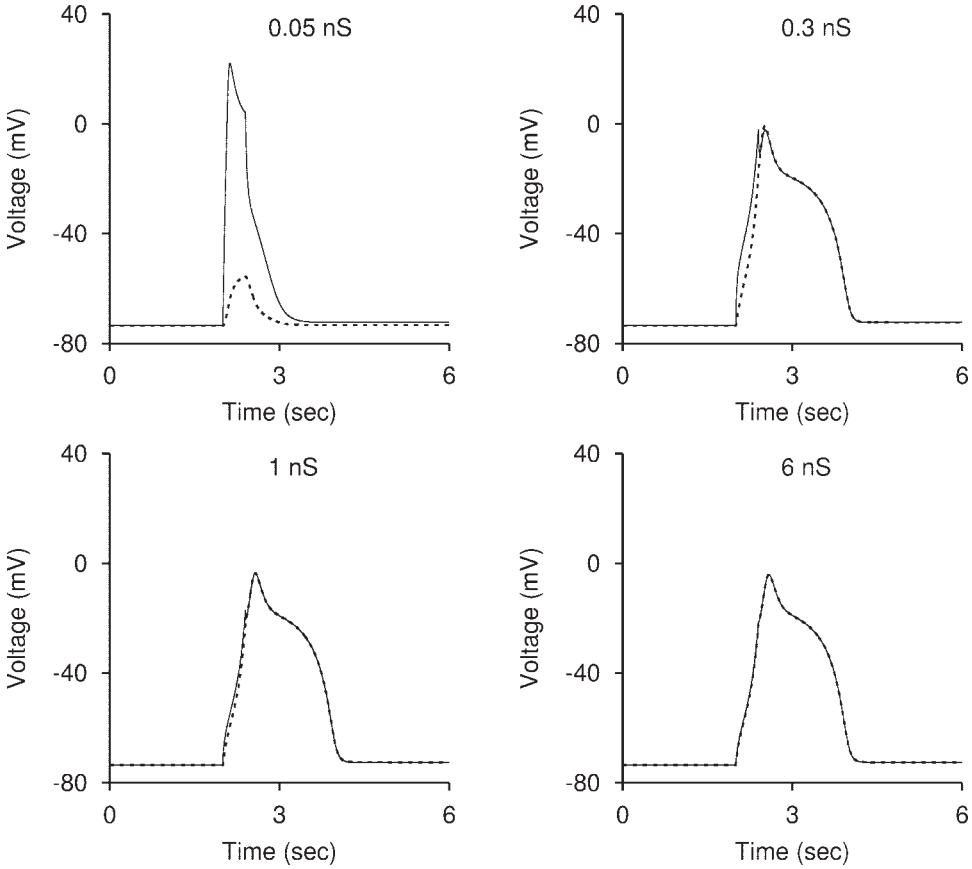

Fig. 10. Current-clamp experiments in a cluster of 7 NRK fibroblast model cells. A current step of 32 pA and 400-ms duration was applied to the center cell, which is coupled with the surrounding 6 cells by gap junctions. Each panel represents the evoked AP recorded in both the center cell of the cluster (solid line) and in 1 of the surrounding cells (dashed line) for 4 different values of the gap junctional strength indicated. Buffer parameters for all cells in the cluster are $T_B = 20\ \mu M$, $k_{on} = 320\ mM^{-1} \cdot s^{-1}$, and $k_{off} = 0.06\ s^{-1}$. Other parameters are as defined in APPENDIX.

obtain AP durations similar to those in NRK monolayer cultures. Over most of the AP time course, the monolayer acts as a whole, except in the sharply rising upstroke of the AP, where the sequential activation time course of the cells around the central area of stimulating cells can be seen. A similar behavior was seen in simulations with a 20 × 20 monolayer size, provided that the central area of stimulating cells was increased. The limited size of the network with its particular network geometry may be expected to produce some border effects in these simulations, e.g., with respect to excitability of the monolayer. Similar border effects may be expected to occur in small monolayer islands of cultured NRK-cells. Thus, with component properties in the physiological range, we could obtain excitability and AP propagation in a relatively small model monolayer. The speed of propagation was in the order of millimeters per second, near that in NRK monolayer cultures (see DISCUSSION).

DISCUSSION

Roles of Various Membrane Conductances

The NRK fibroblast cell model presented in this article is the first model describing the main features for AP generation and propagation in NRK fibroblasts. The model gives insights into the mechanism of AP generation in single cells and AP propagation in small cell clusters and monolayers of electrically coupled NRK cells. The model well reproduces the typical shape of the NRK cell AP with its initial spike and long-duration plateau as well as calcium buffering effects on the shape of the AP. In short, G_{CaL} is responsible for the initial spike and $G_{Cl(Ca)}$ for the plateau of the AP. G_{Kir} is important for the resting membrane potential. APs could be evoked by electrical stimulation with positive current pulses, by external potassium pulses, and by intracellular calcium pulses, all acting by depolarization. In the first two cases, the intracellular calcium transient follows excitation; in the third case, it causes the excitation, as in experiments (2).

The present model is a minimal model, that is, a model of minimal complexity but containing the essential components to produce the qualitative electrical behavior of quiescent NRK cells in isolation and in groups of electrically coupled cells. Apparently, the components of the model and their estimated properties were sufficient to reproduce that qualitative behavior. The model results (see Fig. 4*B*) illustrate that the role of the inward-rectifier channels in NRK cells is multiple. First, they serve to establish, together with a small leak conductance, a resting membrane potential at a high membrane resistance ($R_m > 1\ G\Omega$) so that the resting condition does not require much energy expenditure. Second, G_{Kir} channels serve to contribute to excitability upon depolarizing events by way of their depolarization-induced deactivation. The collapse of G_{Kir} may already occur below the potential of G_{CaL} activation (see Fig. 4*B*) and therefore cause a membrane potential threshold for excitation below the AP of G_{CaL}. Third, the closure of G_{Kir} channels during the AP plateau supports the maintenance of that plateau while at the same time causing minimal energy expenditure for maintaining the ion concentration gradients across the fibroblast membrane. Finally, regenerative activation of G_{Kir} channels upon repolarization (Fig. 4*B*) due to

Downloaded from http://ajpcell.physiology.org/ by 10.220.32.247 on August 31, 2016

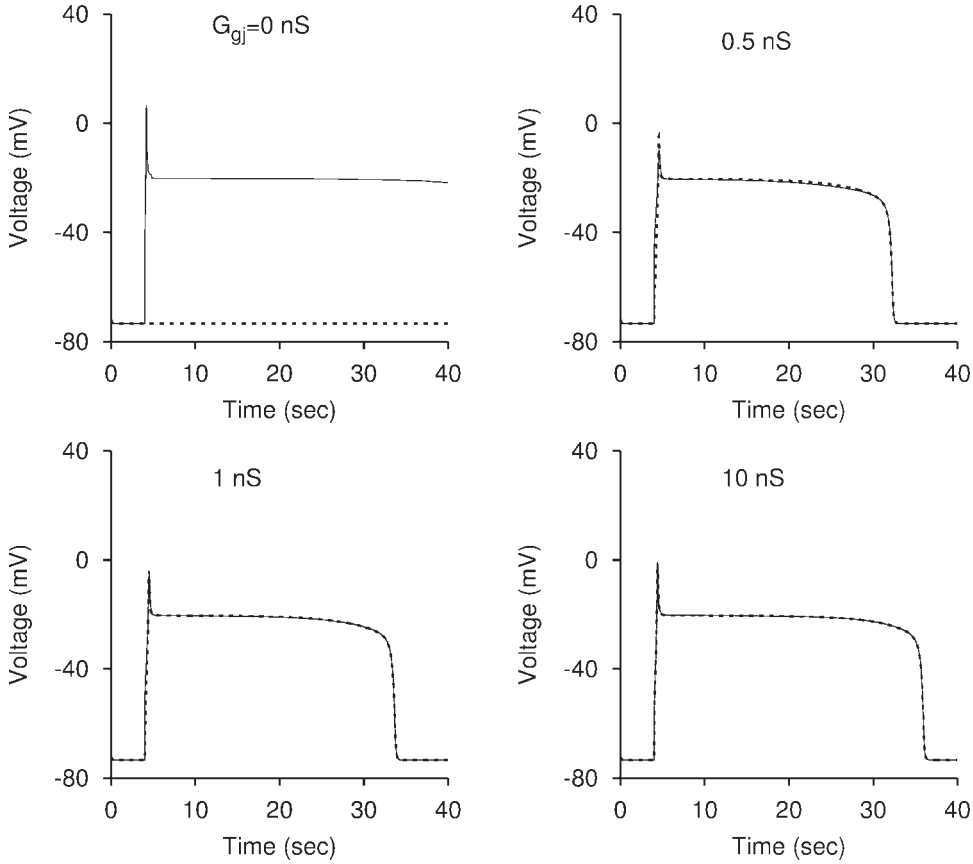

Fig. 11. Excitability of the NRK fibroblast monolayer (7 × 7 cells) by a potassium pulse with strontium in the external medium for increasing gap junctional coupling. This pulse was simulated by changing the V_K from −80 mV to 0 mV in the center region (consisting of 19 cells) of the monolayer over a duration of 800 ms. Each panel represents the synchronization of the electrical responses between the cell in the center of the monolayer (solid line) and the cell at the border of the monolayer (dashed line) for 4 different gap junctional conductances indicated. Intracellular calcium buffering was absent (T_B = 0 μM).

$G_{Cl(Ca)}$ deactivation (following intracellular calcium clearance) contributes to this AP repolarization. These important roles of G_{Kir} channels justify future studies for a further characterization and molecular identification of these channels and on regulation mechanisms of G_{Kir} channel modulation and expression. One improvement of the G_{Kir} model component we used would be to incorporate the dependence of its properties on external potassium concentration (see Ref. 29), which would result in an increased inward-rectifier conductance during an external potassium pulse. A few exploratory simulations in which the G_{Kir} was adapted in this sense indicated that external potassium pulse stimulations were more effective in single cells and monolayers.

In an experimental study in our laboratory (9), Harks et al. observed that only ~30% of the single cells were electrically excitable, whereas small cell clusters were all excitable. We attributed this finding to the relatively large variable leaks in the single cells. We could confirm this interpretation by increasing the leak in a few additional simulations of single-cell stimulation experiments. These simulations also showed the strong sensitivity of NRK cell excitability to changes in the parameters of the various components of the excitability mechanism, in particular those affecting cytoplasmic calcium. This could be due to the fact that some of the parameters had to be estimated because of the lack of experimentally measured values. It could also indicate a physiological lability of the membrane potential and excitability, consistent with other work in our laboratory (8) showing that the resting membrane potential may lie close to the V_K of approximately −80 mV or to the V_{Cl} of approximately −20 mV, dependent on growth conditions affecting cytosolic calcium.

Intracellular Calcium Dynamics

The role of the intracellular calcium dynamics for the control of the long AP duration is unique compared with that in nerve and muscle excitability. The fibroblast AP probably belongs to the longest duration APs (~30 s) in vertebrate excitable cells. Without buffering, the AP duration in the model is very long (>30 s) and only depends on calcium extrusion. With very strong buffering, a very short AP occurs (<2 s) with minimal or no contribution of $I_{Cl(Ca)}$. Similar differences in AP duration with and without strong buffering have been found in patch-clamp experiments on NRK cells (9). However, in real NRK cells, calcium release from intracellular calcium stores may contribute to intracellular calcium dynamics, as suggested by experiments of De Roos et al. (4). Because this calcium release is absent in our model, our model results primarily serve to illustrate the functional importance of intracellular calcium dynamics. Obviously, the relative contribution of calcium buffering and extrusion to AP shaping may be different in real cells if calcium release is present. The model already shows that this internal calcium release is able to cause membrane excitation from within the cell (Figs. 6 and 8).

Another simplification of intracellular calcium dynamics may be the absence of intracellular compartmentalization. For example, the presence of a cytoplasmic shell just beneath the plasma membrane separated by a diffusion barrier from the deeper cytoplasm with calcium release stores (see Ref. 18)

Downloaded from http://ajpcell.physiology.org/ by 10.220.32.247 on August 31, 2016

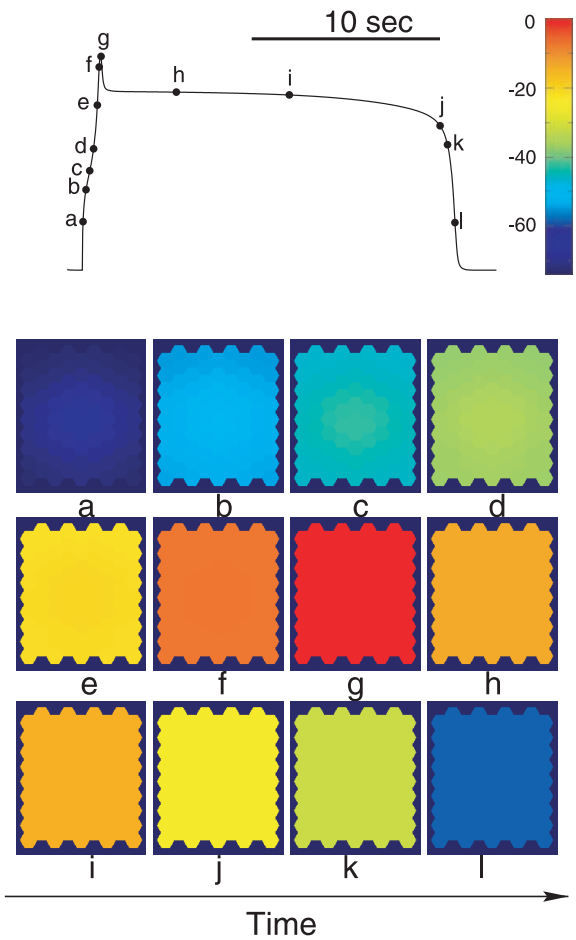

Fig. 12. Consecutive snapshots (*a–l*) in a monolayer of 9 × 9 cells, stimulated as in Fig. 11, showing wave propagation from the center to the border of the monolayer after stimulation with a potassium pulse of 1 s in the center 19 cells of the network. The time intervals between different snapshots were variable, and the pictures were taken at the time points indicated along the AP of the center cell, represented at *top*. The gap junctional coupling among cells was G_{gj} = 6 nS. Buffer conditions were T_B = 9 μM, k_{on} = 320 $mM^{-1}\cdot s^{-1}$. and k_{off} = 0.06 s^{-1}. Other conditions were the same as described in Fig. 11. The blue-to-red scale goes from negative to positive membrane potential (see color calibration bar at *top right*).

would give a different calcium dynamics compared with that of our model with instantaneous single-compartment filling of the cytoplasmic space, with calcium entering only via L-type calcium channels. Such a compartmentalization would affect the way calcium entry would feed back on L-type channels by calcium-induced inactivation and on the time course of inducing calcium release from calcium release stores deeper in the cell.

Considering these questions, it is clear that a realistic modeling of fibroblastic intracellular calcium dynamics requires a detailed experimental characterization of the calcium entry pathways (L-type channels with voltage- and calcium-dependent inactivation, leak of calcium through the membrane, contribution of store-operated calcium channels), intracellular calcium buffering, intracellular calcium release and reuptake, and calcium extrusion from the cells. Modeling the translation of calcium dynamics to $G_{Cl(Ca)}$ activation would require the experimental characterization of the calcium-dependent chloride channels. This would include possible voltage-dependent

Table 1. *Generalized Hodgkin-Huxley-like currents*

Current I_i	V_i, mV	$\bar{G}_i$, nS	m_i	h_i
I_{Kir}	−80	2.2	$\Im(V_m)$	1
I_{CaL}	50	0.5	m	h
$I_{Cl(Ca)}$	−20	10	$\frac{[Ca^{2+}]}{[Ca^{2+}] + K_{Cl(Ca)}}$	1
I_{leak}	0	0.05	1	1

Current I_i is calculated as $\bar{G}_i m_i^p h_i^q (V_m - V_i)$, where $p = q = 1$. See text for definitions.

properties (10, 14), which have been neglected in the present model.

Role of Gap Junctional Coupling

The model results suggest that the degree of gap junctional coupling between an NRK cell and its surrounding cells, where $G_{gj} > 60$ nS (7), is much better than that just required for intercellular AP conduction (cf., Figs. 10 and 11). On the other hand, coupling seems too strong for AP generation in single cells or small areas of cells embedded in the monolayer (Fig. 12). This indicates that fibroblast excitability in culture tends to be a collective property of the cells, requiring, in the case of local stimulation, a sufficient fraction of the whole cell culture to obtain a response of the culture as a whole. The same may hold for the in vivo excitability of the fibroblastic tissue component of an organ, where paracrine mechanisms are responsible for fibroblast activation in maintaining organ integrity, e.g., during wound healing (1).

The model properties also are of interest for the question of the relative importance of electrical conduction of excitation for the propagation of calcium waves in a tissue of cells coupled by gap junctions. Local stimulation signals (e.g., bradykinin) may cause local intracellular calcium transients as well as APs in a monolayer of NRK cells, which are then propagated over the monolayer (2, 4). If the single or spontaneously repeating calcium wave has an intracellular origin, calcium diffusion through gap junctions causing calcium-induced calcium release in neighbor cells might be one mechanism for calcium wave propagation (11). However, calcium buffering and removal recently have been shown to preclude the action of calcium as a purely diffusive gap junctional messenger over many cells and also to limit strongly the velocity of calcium wave propagation from cell to cell (12). In accordance with these theoretical predictions, intracellular calcium waves have been reported to propagate across the tissue at ~5–50 μm/s in the rat liver and blowfly salivary gland (25, 30), whereas in NRK fibroblasts, locally induced calcium APs propagate throughout the monolayer at a velocity as high as ~6 mm/s (2). In the present study, we have shown that these much

Table 2. *Gating variables of I_{CaL}*

Gating Variable x	x_∞	τ_x, s
m	$\frac{1}{1 + e^{-(V_m+10)/6.24}}$	$\frac{m_\infty \cdot 0.01(1 - e^{-(V_m+10)/5.9})}{0.035(V_m + 10)}$
h	$\frac{1}{1 + e^{(V_m+45.06)/8.6}} + \frac{0.8}{1 + e^{0.05(50-V_m)}}$	$\frac{0.01}{0.02 + 0.0197e^{-[0.0337(V_m+10)]^2}}$

Downloaded from http://ajpcell.physiology.org/ by 10.220.32.247 on August 31, 2016

faster calcium waves can be achieved according to a mechanism in which the calcium inflow through L-type calcium channels in one cell triggers an intracellular calcium rise in its neighbor cell. In our model, it is the fast electrotonically propagating calcium AP that precedes the fast calcium wave propagation in monolayers of these cells. The gap junctional conductances required for the fast propagation of calcium APs in the model fall within the range of experimentally determined values for these conductances in NRK fibroblasts.

Limitations and Future Perspective

Although a propagating AP can be simulated with the present model, it has not been possible, so far, to obtain spontaneous repetitive AP firing as observed in density-arrested NRK cells (5). The model predicts that this spontaneous firing does not result from altered expression levels of ion-conducting channels in density-arrested NRK cultures but may involve more complex intracellular calcium dynamics. The present model can easily be extended by introducing more realistic assumptions in the calcium dynamics given in *Eq. 10* [e.g., by including calcium-activated calcium release from the endoplasmic reticulum, calcium pumping via sarco(endo)plasmic reticulum calcium ATPase (SERCA) pumps between cytosol and calcium stores (see Ref. 17), leak of calcium through the cell membrane, and calcium inflow via calcium release-activated calcium channels (CRAC) (23, 26)]. Current research (16) is aimed at resolving the possible role and interplay of intracellular calcium stores in providing the cells a timing mechanism for spontaneous periodic electrical activity (see Ref. 20).

APPENDIX

Mathematical Description of the Ionic Currents

Hodgkin-Huxley-like currents. Table 1 presents gating variables and parameter values of generalized Hodgkin-Huxley-like currents, where $I_i = \bar{G}_i m_i^p h_i^q (V_m - V_i)$, with $p = q = 1$. Table 2 shows equations for gating variables of I_{CaL}.

Other parameters and functions. Actual calculations used to obtain many parameters and functions of the model are listed below.

$$\Im(V_m) = 0.0045 \cdot \exp(-1.489 \cdot V_m \cdot F/RT)/[1 + 0.0045 \cdot \exp(-1.489 \cdot V_m \cdot F/RT)]$$

$$K_d = 0.2\ \mu\text{M}$$

$$V_{pump}^{max} = 1.27 \times 10^{-3}\ \text{mM} \cdot \text{s}^{-1}$$

$$K_{Cl(Ca)} = 35\ \mu\text{M}$$

$$F = 96{,}480\ \text{C/mol}$$

$$C_m = 20\ \text{pF}$$

$$F/RT = 0.0396\ \text{mV}^{-1}$$

$$z_{Ca} = +2$$

$$T = 20°\text{C}$$

$$V_{cell} = 2.1 \times 10^{-12}\ \text{liter}$$

ACKNOWLEDGMENTS

We thank Prof. C. C. A. M. Gielen (Dept. of Medical Physics and Biophysics, University of Nijmegen) for stimulating discussions and support in preparation of this manuscript.

GRANTS

J. J. Torres acknowledges support from the Spanish Ministerio de Ciencia y Tecnología and Fondo Europeo de Desarrollo Regional (Ramón y Cajal contract and project no. BFM2001-2841) and partial support from the University of Granada (Plan Propio de Investigación) and the Dutch Foundation for Neural Networks. D. L. Ypey is supported by the Foundation Nijmegen University Fund.

REFERENCES

1. **Bennett NT and Schultz GS.** Growth factors and wound healing: biochemical properties of growth factors and their receptors. *Am J Surg* 165: 728–737, 1993.
2. **De Roos A, Willems PH, van Zoelen EJ, and Theuvenet AP.** Synchronized Ca^{2+} signaling by intercellular propagation of Ca^{2+} action potentials in NRK fibroblasts. *Am J Physiol Cell Physiol* 273: C1900–C1907, 1997.
3. **De Roos AD, van Zoelen EJ, and Theuvenet AP.** Determination of gap junctional intercellular communication by capacitance measurements. *Pflügers Arch* 431: 556–563, 1996.
4. **De Roos AD, Van Zoelen EJ, and Theuvenet AP.** Membrane depolarization in NRK fibroblasts by bradykinin is mediated by a calcium-dependent chloride conductance. *J Cell Physiol* 170: 166–173, 1997.
5. **De Roos AD, Willems PH, Peters PH, van Zoelen EJ, and Theuvenet AP.** Synchronized calcium spiking resulting from spontaneous calcium action potentials in monolayers of NRK fibroblasts. *Cell Calcium* 22: 195–207, 1997.
6. **Harks EG, Camina JP, Peters PH, Ypey DL, Scheenen WJ, Van Zoelen EJ, and Theuvenet AP.** Besides affecting intracellular calcium signaling, 2-APB reversibly blocks gap junctional coupling in confluent monolayers, thereby allowing the measurement of single-cell membrane currents in undissociated cells. *FASEB J* 17: 941–944, 2003.
7. **Harks EG, De Roos AD, Peters PH, De Haan LH, Brouwer A, Ypey DL, van Zoelen EJ, and Theuvenet AP.** Fenamates: a novel class of reversible gap junction blockers. *J Pharmacol Exp Ther* 298: 1033–1041, 2001.
8. **Harks EG, Peters PH, Dernison MM, Van Dongen JL, Van Zoelen EJ, and Theuvenet AP.** Activation of FP-prostanoid receptors is involved in phenotypic transformation and concomitant depolarization of NRK fibroblasts (Abstract). *Biophys J* 86, *Suppl*: 458a, 2004.
9. **Harks EG, Torres JJ, Cornelisse LN, Ypey DL, and Theuvenet AP.** Ionic basis for excitability of normal rat kidney (NRK) fibroblasts. *J Cell Physiol* 196: 493–503, 2003.
10. **Ho MW, Kaetzel MA, Armstrong DL, and Shears SB.** Regulation of a human chloride channel. A paradigm for integrating input from calcium, type II calmodulin-dependent protein kinase, and inositol 3,4,5,6-tetrakisphosphate. *J Biol Chem* 276: 18673–18680, 2001.
11. **Hofer T.** Model of intercellular calcium oscillations in hepatocytes: synchronization of heterogeneous cells. *Biophys J* 77: 1244–1256, 1999.
12. **Hofer T, Politi A, and Heinrich R.** Intercellular Ca^{2+} wave propagation through gap-junctional Ca^{2+} diffusion: a theoretical study. *Biophys J* 80: 75–87, 2001.
13. **Jinno S, Lin J, Yageta M, and Okayama H.** Oncogenic cell cycle start control. *Mutat Res* 477: 23–29, 2001.
14. **Kidd JF and Thorn P.** The properties of the secretagogue-evoked chloride current in mouse pancreatic acinar cells. *Pflügers Arch* 441: 489–497, 2001.
15. **Koch C.** Biophysics of Computation: Information Processing in Single Neurons. New York: Oxford University Press, 1999.
16. **Kusters JM, Theuvenet AP, Ypey DL, and Gielen CC.** Coupling of action potential firing and Ca-oscillations in a monolayer of gap junctionally coupled NRK fibroblasts. *Biophys J* 86, *Suppl*: 303a, 2004.
17. **Lee HC.** NAADP: an emerging calcium signaling molecule. *J Membr Biol* 173: 1–8, 2000.
18. **Marsault R, Murgia M, Pozzan T, and Rizzuto R.** Domains of high Ca^{2+} beneath the plasma membrane of living A7r5 cells. *EMBO J* 16: 1575–1581, 1997.
19. **Naraghi M.** T-jump study of calcium binding kinetics of calcium chelators. *Cell Calcium* 22: 255–268, 1997.
20. **Patel S, Churchill GC, and Galione A.** Coordination of Ca^{2+} signalling by NAADP. *Trends Biochem Sci* 26: 482–489, 2001.
21. **Postma FR, Hengeveld T, Alblas J, Giepmans BN, Zondag GC, Jalink K, and Moolenaar WH.** Acute loss of cell-cell communication caused by G protein-coupled receptors: a critical role for c-Src. *J Cell Biol* 140: 1199–1209, 1998.

Downloaded from http://ajpcell.physiology.org/ by 10.220.32.247 on August 31, 2016

22. **Puglisi JL and Bers DM.** LabHEART: an interactive computer model of rabbit ventricular myocyte ion channels and Ca transport. *Am J Physiol Cell Physiol* 281: C2049–C2060, 2001.
23. **Putney JW Jr.** A model for receptor-regulated calcium entry. *Cell Calcium* 7: 1–12, 1986.
24. **Rasmusson RL, Clark JW, Giles WR, Shibata EF, and Campbell DL.** A mathematical model of a bullfrog cardiac pacemaker cell. *Am J Physiol Heart Circ Physiol* 259: H352–H369, 1990.
25. **Robb-Gaspers LD and Thomas AP.** Coordination of Ca^{2+} signaling by intercellular propagation of Ca^{2+} waves in the intact liver. *J Biol Chem* 270: 8102–8107, 1995.
26. **Torres JJ, Willems PH, Kappen HJ, and Koopman WJ.** Hysteresis and bistability in a realistic model for IP_3-driven Ca^{2+} oscillations. *Europhys Lett* 55: 746–752, 2001.
27. **Van Zoelen EJ and Tertoolen LG.** Transforming growth factor-β enhances the extent of intercellular communication between normal rat kidney cells. *J Biol Chem* 266: 12075–12081, 1991.
28. **Van Zoelen EJ, van Oostwaard TM, and de Laat SW.** The role of polypeptide growth factors in phenotypic transformation of normal rat kidney cells. *J Biol Chem* 263: 64–68, 1988.
29. **Wallinga W, Meijer SL, Alberink MJ, Vliek M, Wienk ED, and Ypey DL.** Modelling action potentials and membrane currents of mammalian skeletal muscle fibres in coherence with potassium concentration changes in the T-tubular system. *Eur Biophys J* 28: 317–329, 1999.
30. **Zimmermann B and Walz B.** The mechanism mediating regenerative intercellular Ca^{2+} waves in the blowfly salivary gland. *EMBO J* 18: 3222–3231, 1999.

Downloaded from http://ajpcell.physiology.org/ by 10.220.32.247 on August 31, 2016